

Warm-started Semionline Trajectory Planner for Ship's Automatic Docking (Berthing)

Dimas M. Rachman^{a,*}, Atsuo Maki^a, Yoshiki Miyauchi^a and Naoya Umeda^a

^aOsaka University, 2-1 Yamadaoka, Suita, 565-0871, Osaka, Japan

ARTICLE INFO

Keywords:
 Automatic docking
 Warm-started optimization
 Trajectory optimization
 Semionline trajectory planner

ABSTRACT

In the usual framework of control, a reference trajectory is needed as the set point for a feedback controller. This leads to a problem on how to scientifically generate the reference trajectory. Such a problem is termed trajectory optimization which is done in a trajectory planner. It is desired that this reference trajectory is kept feasible with respect to the ship's dynamics, the dynamics of the environment (wind), and the surrounding boundary. For an underactuated conventional vessel, its mathematical model can be very intricate. This causes significant computational time. This article demonstrates that the balance between the feasibility of the reference trajectory and the computational time can be achieved for an underactuated vessel in a disturbed and restricted environment. This is done by: (1) using an almost-global offline solution as a warm start in a semionline trajectory optimization to speed up the calculation, (2) including the prediction of wind dynamics, and (3) using a predefined boundary to generate the necessary spatial constraints that guarantee a collision-free trajectory. Incorporation of these three things results in a feasible and safe trajectory, with a considerable computational time speedup. In addition, the warm start generally gives better results than that without warm start.

1. Introduction

One of the most discussed matters in the problem of automatic docking is the trajectory planning of the docking operation. Usually, a trajectory is planned through *trajectory optimization*, which is a case of continuous optimal control problem (OCP). Practically a continuous OCP is discretized and transcribed into a finite-dimensional nonlinear optimization problem (NLP) via *direct* methods such as *shooting* method and *collocation* method. In this article, the term OCP is used interchangeably with trajectory optimization.

Trajectory planner for a docking operation is quite different from that for a general operation. The global nature of a general operation makes it possible for the trajectory to be obtained by smoothing a path in accordance to part of the ship's dynamics (Vagale et al., 2021; Zhou et al., 2020). However, when planning a trajectory for a docking operation, the low speed and high safety requirement result in a more complicated dynamics and subsequently the trajectory optimization itself.

Research on trajectory planner for docking operation sees various efforts to balance three things: low computational cost (Bitar et al., 2020; Martinsen et al., 2020), applicability to underactuated conventional vessel (Maki et al., 2021, 2020; Mizuno et al., 2015), and feasibility with respect to the surrounding dynamic (Han et al., 2021; Mizuno et al., 2015) and geometric information (Bitar et al., 2020; Liao et al., 2019; Martinsen et al., 2019; Miyauchi et al., 2021b). This is relevant, because in practice a shipmaster will try to replan a new trajectory for docking operation if it is considered not feasible anymore. Even an experienced shipmaster might require some time to plan a new trajectory.

For this reason, to realize an autonomous ship, it is necessary to design a relatively fast planner that can replan a feasible and safe trajectory, and applicable to conventional vessel.

This article limits the discussion within the scope of OCP-based trajectory planner that was pioneered by Shouji et al. (1992). The trajectory planner introduced in Maki et al. (2021) and Miyauchi et al. (2021b) can produce an almost-global, feasible, and safe trajectory for a conventional vessel, but requires long computational time. The one introduced in Mizuno et al. (2015) is relatively fast and also applicable to conventional vessel, but there are no spatial constraints that can guarantee safe trajectory. On the other hand, Martinsen et al. (2020) showed a fast planner that guarantee a safe trajectory, but applicable for a fully/overly actuated vessel.

By exploiting the advantages of the previously mentioned works, the main intention of this article is to introduce a *semionline trajectory planner* (SO-TP) that is able to plan a collision-free trajectory for an underactuated vessel under wind disturbance. The term *semionline* implies the ability of the planner to take into account the wind dynamics measured on the vessel when the planner is executed.

One of the key points in this SO-TP is to use the almost-global and feasible solution from Maki et al. (2021) as a *warm start*, i.e., good initial guess in the SO-TP. To evaluate its performance, the following matters are discussed:

1. The applicability of just one warm start to speed up the SO-TP for various scenarios: different initial states and wind parameters.
2. The comparison of the resulting trajectories with and without warm start (linear initial guess). Results from a total of 14 different scenarios are compared based on the feasibility and the computational time.
3. The comparison of the resulting trajectories with two different warm starts: (1) obtained by the method in

*Corresponding author

Email address: dimas_rachman@naoe.eng.osaka-u.ac.jp (D.M. Rachman)

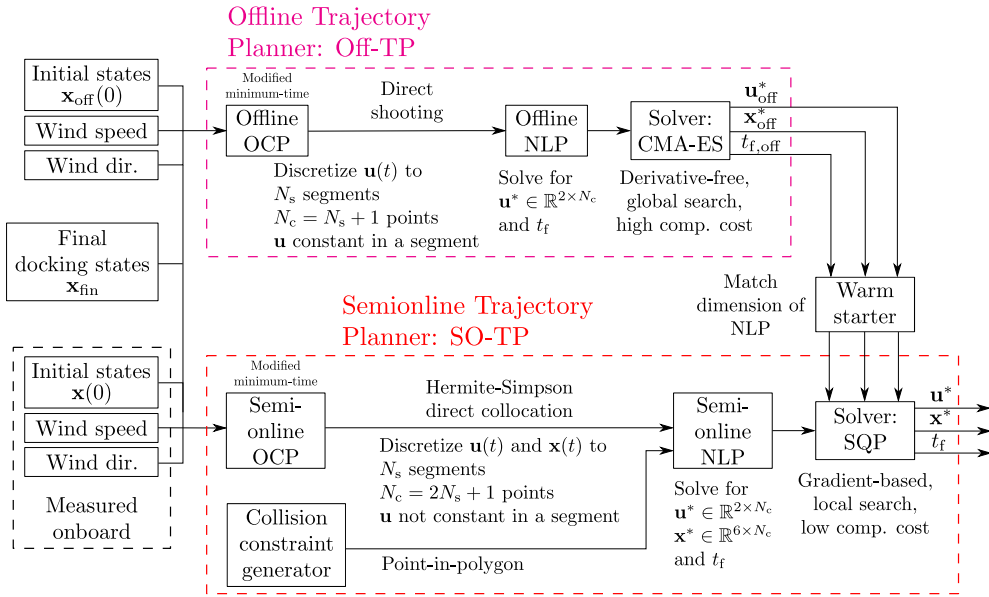


Fig. 1: Outlines of the warm-started semionline trajectory planner.

Maki et al. (2021); (2) obtained by the SO-TP with linear initial guess. This is to show the necessity for the almost-globally optimal solution as the warm start.

The readers will find this article as a continuation and implementation of the work in Maki et al. (2021).

2. Proposed Scheme and Formulation

The outlines of the proposed scheme is visualized in Fig. 1 and can be summarized into the following steps:

1. First, optimal trajectories are generated. These optimal trajectories are termed *offline trajectories* or *offline solutions*, and the planner is called *offline trajectory planner* (abbreviated as Off-TP).
2. The offline solutions can be obtained for several initial states and wind parameters. As a demonstration, this article shows how just one offline solution (without considering the wind) can be used in many scenarios.
3. Then, the offline solution is used to warm-start the semionline trajectory planner (SO-TP).
4. The OCP in the SO-TP is discretized and transcribed into a finite-dimensional NLP by direct Hermite-Simpson collocation method. The form of the objective function is identical to that in the Off-TP.
5. With a *point-in-polygon* algorithm, one can check whether a point is inside or outside a polygon that defines an obstacle-free region. This results in several nonlinear and implicit spatial constraints to the NLP.
6. Finally, the online NLP is solved by MATLAB `fmincon` package with SQP (*sequential quadratic programming*) (Boggs and Tolle, 1995) as its main algorithm. An optimization where a good guess is provided is called a *warm-started* optimization (Forsgren, 2006).

In this article, the trajectory planner is simulated for an underactuated tanker: a 3 m *Esso Osaka* 1/108 scale model or just *Esso Osaka* (the principal particulars are given in Table A.1 in the appendix). She is equipped with an electric motor that allows instantaneous mode switch and single rudder that can rotate at a rate of approximately 70 degree/s.

2.1. Esso Osaka Maneuvering Model

Normally a docking operation is carried out at a low surge velocity. For an underactuated conventional vessel: nonholonomic, it usually requires the dynamics for all possible combinations of surge velocity and propeller's modes to be described. For these reasons, the mathematical model of such a system can be very nonlinear and intricate.

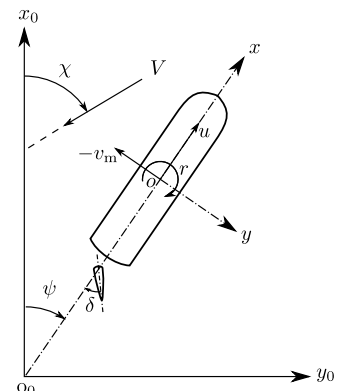


Fig. 2: Coordinate systems.

Two coordinate systems are introduced: a ship-fixed coordinate system $o - xy$ where midship is its origin and an earth-fixed coordinate system $o_0 - x_0y_0$. Angle between the two coordinate systems is the ship's yaw angle ψ and r

denotes its angular velocity. The surge and sway velocities at the midship are denoted by u and v_m , respectively.

The kinematics at the midship can be transformed from the ship-fixed coordinate system to the earth-fixed coordinate system by the following transformation,

$$\frac{d}{dt} \begin{Bmatrix} x_0 \\ y_0 \\ \psi \end{Bmatrix} = \begin{bmatrix} \cos \psi & -\sin \psi & 0 \\ \sin \psi & \cos \psi & 0 \\ 0 & 0 & 1 \end{bmatrix} \begin{Bmatrix} u \\ v_m \\ r \end{Bmatrix}. \quad (1)$$

The kinetics of Esso Osaka is based on the standard equations of motion presented by the MMG (maneuvering model group) (Yasukawa and Yoshimura, 2014) as follows:

$$(m + m_x) \dot{u} - (m + m_y) v_m r - x_G m r^2 = X \quad (2a)$$

$$(m + m_y) \dot{v}_m + (m + m_x) u r + x_G m \dot{r} = Y \quad (2b)$$

$$(I_{zG} + x_G^2 m + J_z) \dot{r} + x_G m (\dot{v}_m + u r) = N_m, \quad (2c)$$

and can be rearranged into,

$$\dot{u} = \frac{X + M_y v_m r + x_G m r^2}{M_x} \quad (3a)$$

$$\dot{v}_m = \frac{(Y - M_x u r) I_{zm} - (N_m - x_G m u r) x_G m}{M_y I_{zm} - (x_G m)^2} \quad (3b)$$

$$\dot{r} = \frac{(Y - M_x u r) x_G m - (N_m - x_G m u r) M_y}{(x_G m)^2 - M_y I_{zm}}, \quad (3c)$$

where simplified terms: $M_x = m + m_x$, $M_y = m + m_y$, and $I_{zm} = I_{zG} + x_G^2 m + J_z$ are used. Here, m and I_{zG} denote the ship's mass and moment of inertia about center of gravity x_G . Moreover, m_x , m_y , and J_z denote the added mass and moment of inertia in each axis.

X and Y are the total surge and sway force, respectively, while N_m is the total moment about the midship. These total forces are contributions from hull forces (Yoshimura et al., 2009), four-quadrant steering and thrust forces (Kitagawa et al., 2015; Miyauchi et al., 2021a; Yasukawa and Yoshimura, 2014), and wind forces (Fujiwara et al., 1998). The important coefficients are given in Maki et al. (2020) and Miyauchi et al. (2021a).

Combining the kinematics (1) and the kinetics, (3) one can obtain the dynamics that can be rearranged into a simplified expression,

$$\dot{\mathbf{x}}(t) = \mathbf{f}(\mathbf{x}(t), \mathbf{u}(t), V, \chi), \quad (4)$$

where V is the true wind speed that *blows-from* at an angle χ from the North (the positive x_0 axis), and

$$\mathbf{x}(t) \triangleq \{ x_0 \ u \ y_0 \ v_m \ \psi \ r \ }^T \quad (5)$$

$$\mathbf{u}(t) \triangleq \{ \delta \ n \ }^T. \quad (6)$$

$\mathbf{x}(t) \in \mathbb{R}^6$ is termed *states* and $\mathbf{u}(t) \in \mathbb{R}^2$ is termed *control*, where δ is rudder angle in degree and n is propeller revolution number in rps (1/s).

2.2. Offline Trajectory Planner: Off-TP

The Off-TP is an OCP-based trajectory planner which goal is to provide a *warm start*, i.e., an almost-globally optimal solution (Forsgren, 2006), as the initial guess to the SO-TP so that it can converge faster. The warm start does not necessarily need to be the solution to the exact same optimization problem.

In the Off-TP, the OCP is discretized and transcribed into a finite-dimensional NLP by shooting method. The goal is to find the optimal control $\mathbf{u}_{\text{off}}^*$ at each discretization point that drive the system from the initial states $\mathbf{x}(0)$ to the desired final docking states \mathbf{x}_{fin} . This optimal control gives optimal state trajectories $\mathbf{x}_{\text{off}}^*$ that minimize a modified minimum-time objective function: gives the optimal final time $t_{f,\text{off}}$. These offline solutions from the Off-TP: $\mathbf{u}_{\text{off}}^*$, $\mathbf{x}_{\text{off}}^*$, and $t_{f,\text{off}}$ are used as a warm start for the SO-TP (see Fig. 1).

The offline NLP is solved by a nonconvex and derivative-free global optimization technique known as the evolution strategy with covariance matrix adaptation (CMA-ES) (Hansen et al., 2003; Auger and Hansen, 2005; Sakamoto and Akimoto, 2017). Despite being computationally demanding (a stochastic technique, coupled with explicit integration of the dynamics and single shooting method), it performed very well to locate the best approximation of the global optimum. So, the offline solution from the Off-TP can be considered almost-globally optimal. Details about the Off-TP are explained in Maki et al. (2021).

2.3. Semionline Trajectory Planner: SO-TP

The SO-TP is developed upon the idea that in practice there may be a need to *replan* the trajectory based on the surrounding conditions. It is desired that the updated trajectory is kept feasible to be tracked by the feedback controller.

Let \bar{t}_j be the j -th sampling of the actual time \bar{t} outside the SO-TP. Let t be the normalized prediction time inside the SO-TP such that $t = 0$ is \bar{t}_j . Then, the continuous (a modified minimum-time OCP, before transcription) semionline trajectory optimization problem at \bar{t}_j can be stated as:

determine $\delta^*, \mathbf{n}^*, t_f$

$$\text{that min. } J_{\text{on}} = \sum_{i=1}^6 (x_i(t_f) - x_{\text{fin},i})^2 \times \int_0^{t_f} \sum_{i=1}^6 (x_i(t) - x_{\text{fin},i})^2 dt \quad (7a)$$

subject to $\dot{\mathbf{x}}(t) = \mathbf{f}(\mathbf{x}(t), \mathbf{u}(t), V(\bar{t}_j), \chi(\bar{t}_j))$, (7b)

$$\mathbf{x}^*(0) = \mathbf{x}(\bar{t}_j), \mathbf{x}^*(t_f) = \mathbf{x}_{\text{fin}}, \quad (7c)$$

$$-\delta_{\text{max}} \leq \delta(t) \leq \delta_{\text{max}}, \quad (7d)$$

$$-n_{\text{max}} \leq n(t) \leq n_{\text{max}}, \quad (7e)$$

$$t \in [0, t_f], \text{ and } t_f \in (0, \infty).$$

The wind parameters are assumed constant when planning the trajectory, i.e., $V(t) = V(\bar{t}_j)$ and $\chi(t) = \chi(\bar{t}_j)$ for all t . Note that this online OCP is similar to that in the Off-TP.

It is practical to plan a reference trajectory that is "easy" to track, i.e., with less control effort. This is to compensate for the uncertainties that may affect the feedback controller. It can be done either by: adding control cost in the objective function (7a) or explicitly limiting the allowable control (to δ_{\max} and n_{\max}). The latter is preferable since it is binding in its box constraint form: (7d) and (7e), see Table 1.

Table 1

Control limitations in generating the reference trajectory.

Control	Limiting values	Actual capacity
δ (deg)	$\delta_{\max} = 25$	35
n (rps)	$n_{\max} = 15$	20

2.3.1. Separated Hermite-Simpson Collocation

The continuous OCP in (7) can be discretized and transcribed into a finite-dimensional nonlinear optimization problem (NLP) by direct collocation. The dynamics, the state, and the control trajectories are discretized into $N_s \in \mathbb{N}$ equal-spaced segments; each bounded by *knot* points.

In *separated* Hermite-Simpson collocation method (Betts, 2010), an additional *collocation* point at the mid-segment is required so that the number of *discretization points* is $N_c = 2N_s + 1$. The true state trajectory in a segment is approximated by first-order third-degree (cubic) *Hermite interpolation polynomial* \mathbf{x}_H with C^1 continuity. On the other hand, the true control trajectory in a segment can be approximated by quadratic, linear, or constant function \mathbf{u}_H . In addition, the integration of the dynamics in a segment is approximated by Simpson quadrature rule, hence the name of the method.

In summary, at each segment there are two additional constraints for the NLP, i.e., the Simpson quadrature constraint and the Hermite interpolation constraint; both imposed at the mid-segment point. The goal of the NLP is to find the optimal control and the optimal states at all discretization points: the knot and the mid-segment points.

2.3.2. Point-in-Polygon: Collision Constraints

Suppose $\mathbf{P}_b \in \mathbb{R}^{2 \times n_v}$ is a matrix whose columns are the vertices position in the earth-fixed coordinate system,

$$\mathbf{P}_b \triangleq \begin{bmatrix} \mathbf{p}_{b,1} & \mathbf{p}_{b,2} & \dots & \mathbf{p}_{b,n_v} \end{bmatrix},$$

where $\mathbf{p}_b = \{x_b \ y_b\}^T$. The number of the vertices, $n_v \geq 3$ is necessary to form a simple polygon: a closed region.

Let $\mathbf{p}_s = \{x_s \ y_s\}^T$ be the point to be checked. If \mathbf{p}_s is inside the polygon formed by \mathbf{P}_b , then the sum of angle between all pairs of lines formed by \mathbf{p}_s and two adjacent polygon vertices, i.e., $\mathbf{p}_{b,i}$ and $\mathbf{p}_{b,i+1}$, must be equal to 2π . If this is not true, then \mathbf{p}_s is outside the polygon. From Fig. 3, let $\theta_{s,i}$ be the angle between two adjacent lines.

Suppose now $\mathbf{P}_s \in \mathbb{R}^{2 \times n_s}$ is a matrix whose columns are the points of the ship's boundary in the earth-fixed

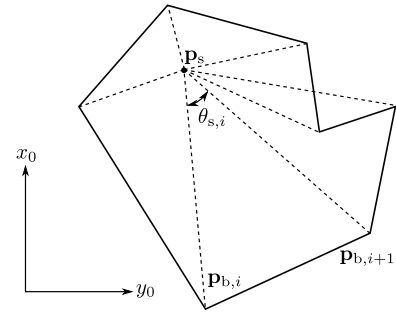


Fig. 3: Sum of all $\theta_{s,i}$ (for $i = 1, \dots, n_v$) must be equal to 2π for point \mathbf{p}_s to be inside the polygon.

coordinate system,

$$\mathbf{P}_s \triangleq \begin{bmatrix} \mathbf{p}_{s,1} & \mathbf{p}_{s,2} & \dots & \mathbf{p}_{s,n_s} \end{bmatrix},$$

where n_s is the number of the ship's boundary points (not to be confused with the discretization points in the collocation). These points depend on the position of midship (x_0, y_0) and the yaw angle (ψ), i.e., some of the optimization variables. Due to this dependency and the requirement that the sum of angle is equal to 2π , one can construct additional equality constraints for the NLP as follows:

$$\sum_{i=1}^{n_v} \theta_{s,i} \Big|_{j,k} = 2\pi. \quad (8)$$

This means that at each discretization point $k = 1, \dots, N_c$, (8) must be evaluated for all ship's boundary points $j = 1, \dots, n_s$. This results in $n_s \times N_c$ equalities.

This method is equivalent to *winding number* method (Hormann and Agathos, 2001) and known as *angle summation* method. In CAD, It is not considered the best method to check whether a point is inside or outside a polygon. Nevertheless, in the scope of this article, it can be regarded as one of the most practical: analytically differentiable and can handle any shape of the harbor area.

2.3.3. Transcribed OCP in the SO-TP

Let t_k be the time at the k -th discretization point (the knot points and the mid-segment points) such that $k = 1, \dots, N_c$. Odd k denote the knot points and even k denote the mid-segment points. The length between two discretization points is $h_{kn} = t_{k+1} - t_k = 0.5h_s$ and the length between two knot points (length of a segment) is $h_s = t_f - t_0$. In this notation, the online OCP (7) can be transcribed to:

determine $\delta_1^*, \delta_2^*, \dots, \delta_{N_c}^* \in \mathbb{R}$,

$n_1^*, n_2^*, \dots, n_{N_c}^* \in \mathbb{R}$,

$\mathbf{x}_1^*, \mathbf{x}_2^*, \dots, \mathbf{x}_{N_c}^* \in \mathbb{R}^6$, $t_f \in \mathbb{R}$

that min. $J_{\text{on}} = \sum_{i=1}^6 (x_i(t_f) - x_{\text{fin},i})^2$

$$\times \int_0^{t_f} \sum_{i=1}^6 (x_i(t) - x_{\text{fin},i})^2 dt \quad (9a)$$

subject to

$$\mathbf{x}_1^* = \mathbf{x}(\bar{t}_j), \mathbf{x}_{N_c}^* = \mathbf{x}_{\text{fin}}, \quad (9b)$$

$$\mathbf{x}_{N_c-2} = \mathbf{x}_{\text{fin}} - \frac{h_s}{6} (\mathbf{f}_{N_c-2} + 4\mathbf{f}_{N_c-1} + \mathbf{f}_{N_c}), \quad (9c)$$

$$\mathbf{x}_H(t_k) = \mathbf{x}_k, \{k \in \mathbb{E} \mid 2 \leq k < N_c\} \quad (9d)$$

$$\mathbf{f}_H(t_k) = \mathbf{f}_k, \{k \in \mathbb{E} \mid 2 \leq k < N_c\} \quad (9e)$$

$$\sum_{i=1}^{n_v} \theta_{s,i} \Big|_{j,k} = 2\pi, \quad j = 1, \dots, n_s \quad (9f)$$

$$-\delta_{\max} \leq \delta(t_k) \leq \delta_{\max}, \quad (9g)$$

$$-n_{\max} \leq n(t_k) \leq n_{\max}, \text{ and} \quad (9h)$$

$$t_f \text{ in } (0, \infty).$$

The integral term in the objective function (9a) is approximated by Simpson quadrature.

The goal of the NLP (9) is to find $(2 + 6)N_c + 1$ number of optimal variables that minimize the objective function (9a). The 6×2 equalities in (9b) and (9c) enforce the initial and final state constraints, while (9d) and (9e) are the $6 \times N_s$ interpolation constraints and $6 \times N_s$ quadrature constraints at the mid-segment, respectively. The $n_s \times N_c$ equalities in (9f) are the collision constraints and the last two box constraints: (9g) and (9h) saturate the control to the given values.

Sequential quadratic programming (SQP) from MATLAB `fmincon` package is used to solve the NLP (9). It is a Newton's method with quadratic local convergence rate (Boggs and Tolle, 1995). With a good initial guess (warm start), less iterations are expected, resulting in a faster convergence to the local optimum.

The next chapter shows how just one offline solution from the Off-TP $(\mathbf{x}_{\text{off}}^*, \mathbf{u}_{\text{off}}^*, t_{f,\text{off}})$ for a no-wind condition can be used to warm-start the SO-TP in various situations.

3. Simulation Conditions

The offline solutions $\mathbf{x}_{\text{off}}^*$ and $\mathbf{u}_{\text{off}}^*$ are obtained by the Off-TP with $V = 0$ and $\chi = 0$ (no wind). The initial states $\mathbf{x}_{\text{off}}^*(0)$, the desired final states \mathbf{x}_{fin} , and the final states $\mathbf{x}_{\text{off}}^*(t_{f,\text{off}})$ of this offline solution are as follows:

$$\mathbf{x}_{\text{off}}^*(0) = \{ 16.50 \ 0.12 \ -7.50 \ 0.00 \ 2\pi/3 \ 0.00 \}^T$$

$$\mathbf{x}_{\text{fin}} = \{ -0.50 \ 0.01 \ -0.50 \ 0.00 \ \pi \ 0.00 \}^T$$

$$\mathbf{x}_{\text{off}}^*(t_{f,\text{off}}) = \{ -0.51 \ 0.01 \ -0.51 \ 0.00 \ 3.14 \ 0.00 \}^T.$$

The performance of the warm-started SO-TP is evaluated for four main situations (M1 to M4) and ten additional trial cases (A1 to A10, see Table 2). The initial states for each cases are expressed as $x_i(\bar{t}_j) = d_i x_{\text{off},i}^*$ for $i = 1, \dots, 6$, where d_i is the element of a vector of multipliers \mathbf{d} . To quantify "how different" the initial states are from $\mathbf{x}_{\text{off}}^*(0)$,

the Euclidean norm is introduced as,

$$L = \sqrt{\sum_i^6 \left[(x_i(\bar{t}_j) - x_{\text{off},i}^*(0)) / x_{\text{off},i}^*(0) \right]^2} = \sqrt{\sum_i^6 (d_i - 1)^2}. \quad (10)$$

3.1. Spatial Constraints Definition

The docking is simulated in the Inukai experiment pond that belongs to Osaka University. The predefined obstacle-free region formed by a simple polygon \mathbf{P}_b is shown in Fig. 4a, with number of vertices $n_v = 11$. The origin of the earth-fixed coordinate system $o_0 - x_0 y_0$ is located at $\mathbf{p}_{b,1}$.

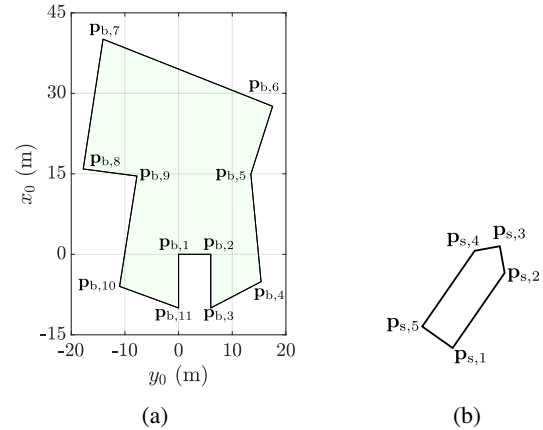


Fig. 4: (a) Shaded region is the obstacle-free region, formed by polygon \mathbf{P}_b with $n_v = 11$ vertices (b) The points of the ship's boundary \mathbf{P}_s with $n_s = 5$ points.

The number of the points of the ship's boundary n_s must be chosen carefully. Adding more points will guarantee a safer trajectory but will increase the number of constraints and the computational time. In the simulation, $n_s = 5$ is considered sufficient as shown in Fig. 4b.

3.2. On the Discretization and Interpolation

The whole trajectory is divided into $N_s = 20$ equal-spaced segments so that the number of discretization points is $N_c = 41$. Upon solving for the optimal control and states at each discretization point, it is necessary to interpolate the values between those points. Unlike in the offline OCP, here the control trajectory in a segment is not constant.

For practical consideration (mechanical limitation of the vessel's actuators), it is assumed that the control trajectory between two consecutive discretization points (half segment) is linear and can be computed as,

$$\mathbf{u}_H^*(t) = \mathbf{u}_k^* + (\mathbf{u}_{k+1}^* - \mathbf{u}_k^*) \frac{t - t_k}{h_{kn}}, \quad (11)$$

for $t \in [t_k, t_{k+1}]$ and $h_{kn} = 0.5h_s$ is the length between two consecutive discretization points.

Table 2

Evaluation cases for the SO-TP, see Fig. A.1 to Fig. A.3 in the appendix.

Case	Multiplier \mathbf{d} $x_i(\bar{t}_j) = d_i x_{\text{off},i}^*(0)$	Initial velocity $u(0)$		$\psi(0)$	$V(\bar{t}_j)$	$\chi(\bar{t}_j)$	Norm $L = \sqrt{\sum_i^6 (d_i - 1)^2}$
		(m/s)	Full scale (knots)				
M1	{ 1.0 1.0 1.0 1.0 1.0 1.0 } ^T	0.12	2.43	$2\pi/3$	No wind		0.00
M2	{ 1.1 2.0 1.1 1.0 1.2 1.0 } ^T	0.24	4.86	$4\pi/5$	0.75	45	1.03
M3	{ 0.9 2.0 0.8 1.0 0.9 1.0 } ^T	0.24	4.86	$3\pi/5$	0.50	225	1.03
M4	{ 1.0 3.0 0.9 1.0 1.5 1.0 } ^T	0.36	7.26	π	0.75	45	2.06
A1	{ 1.2 1.2 1.1 1.0 1.1 1.0 } ^T	0.14	2.91	$11\pi/15$	0.75	45	0.32
A2	{ 1.2 1.4 1.2 1.0 1.2 1.0 } ^T	0.17	3.40	$4\pi/5$	0.75	180	0.53
A3	{ 1.3 1.6 0.9 1.0 1.4 1.0 } ^T	0.19	3.88	$14\pi/15$	0.75	125	0.79
A4	{ 1.4 1.8 0.8 1.0 0.9 1.0 } ^T	0.22	4.37	$3\pi/5$	0.50	135	0.92
A5	{ 1.5 0.8 1.2 1.0 1.1 1.0 } ^T	0.09	1.94	$11\pi/15$	0.50	90	0.58
A6	{ 1.0 0.8 0.7 1.0 1.2 1.0 } ^T	0.09	1.94	$4\pi/5$	0.50	315	0.41
A7	{ 1.2 2.2 0.8 1.0 0.8 1.0 } ^T	0.26	5.34	$8\pi/15$	0.50	250	1.25
A8	{ 1.2 2.0 0.0 1.0 1.5 1.0 } ^T	0.24	4.86	π	0.50	90	1.51
A9	{ 1.0 1.0 -1.0 1.0 2.0 1.0 } ^T	0.12	2.43	$4\pi/3$	0.75	0	2.24
A10	{ 0.8 1.5 -0.9 1.0 2.2 1.0 } ^T	0.18	3.64	$22\pi/15$	0.50	45	2.31

The state trajectory in a segment is interpolated by *natural cubic spline interpolation* method (Press et al., 1992). It retains the same accuracy $O(h_s^4)$ of Hermite cubic interpolation with C^2 continuity. The resulting natural cubic spline interpolant within a segment $[t_k, t_{k+2}]$ can be written as,

$$\mathbf{x}_H^*(t) = \mathbf{x}_k^* + \mathbf{f}_k^* \tau - \left(3\mathbf{f}_k^* - 4\mathbf{f}_{k+1}^* + \mathbf{f}_{k+2}^* \right) \frac{\tau^2}{2h_s} + \left(2\mathbf{f}_k^* - 4\mathbf{f}_{k+1}^* + 2\mathbf{f}_{k+2}^* \right) \frac{\tau^3}{3h_s^2}, \quad (12)$$

for every odd k in $1 \leq k \leq N_c - 2$ and $\tau = t - t_k$. Here $\mathbf{f}_k^* \triangleq \mathbf{f}(\mathbf{x}_k^*, \mathbf{u}_k^*, V(\bar{t}_j), \chi(\bar{t}_j))$ is the true dynamics evaluated at odd k (knot points).

4. Simulation Results and Evaluation

This section discusses the performance of the SO-TP. The simulations are done on a laptop with 16GB RAM and 8-core processor.

4.1. Main Cases: Examples

The main cases M1 to M4 are intended to give some examples of how just one almost-global and feasible solution of a slightly different problem from the Off-TP can be used as a warm start for different situations in the SO-TP (adhere to the first evaluation matter), see Table 2. Note that the Off-TP and the SO-TP differ in the OCP transcription method, the form of the objective function, and how the control trajectory is assumed within a segment.

Now, to emphasize the advantages of the warm start to the SO-TP, it is relevant to show the results of the SO-TP without warm start. Without warm start, a linear guess is

provided, i.e., linearly changing from the initial states to the desired final states. Meanwhile, the initial guess for the control is constant: $0.5\delta_{\max}$ and $0.5n_{\max}$. The initial guess of the final time t_f is 160 s, equal to that of the warm start.

4.1.1. Case M1: No Wind + Same Initial States

This case is intended to confirm whether the SO-TP converges to the same warm start or not, with the same condition which the warm start was solved, i.e., no wind and same initial states (see section 3). The comparison between the optimal control and state trajectories obtained by the SO-TP with and without warm start for this case are shown in Fig. 5 and Fig. 6. In the figures, the CMA-ES guess means the warm start from the Off-TP.

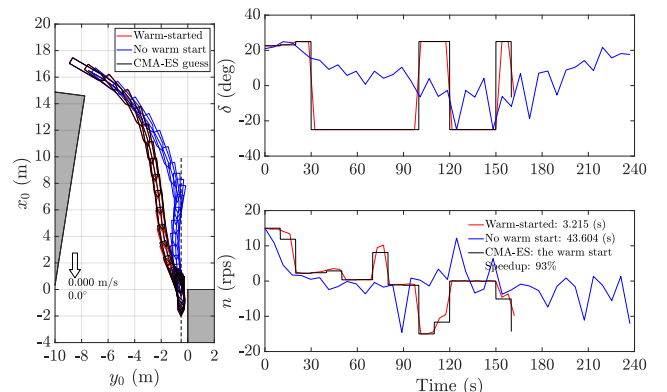


Fig. 5: Case M1: summary and optimal control trajectories, no wind, with 3.215 s calculation time.

The SO-TP converged to the solution that is almost similar to the provided warm start in a relatively fast computational time. This is a clear and direct demonstration that despite the OCP in the Off-TP is formulated differently in almost all aspects, its solution belongs to the feasible set of the OCP in the SO-TP (7a).

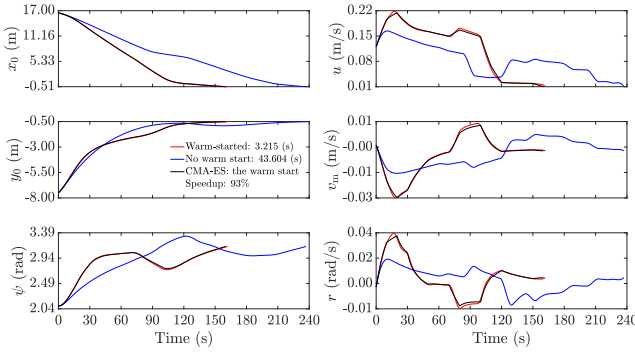


Fig. 6: Case M1: optimal state trajectories, no wind, with 3.215 s calculation time.

4.1.2. Case M2: Wind Blows Away from the Berth + Farther Initial States

In this case, the SO-TP is executed with initial positions farther from the berth. The initial surge velocity is doubled $u(0) = 2u_{\text{off}}(0)$ and the initial yaw angle is less-sharp against the berth. The wind blows at 0.75 m/s from 45 degree, away from the berth. The resulting optimal control and state trajectories are shown in Fig. 7 and Fig. 8.

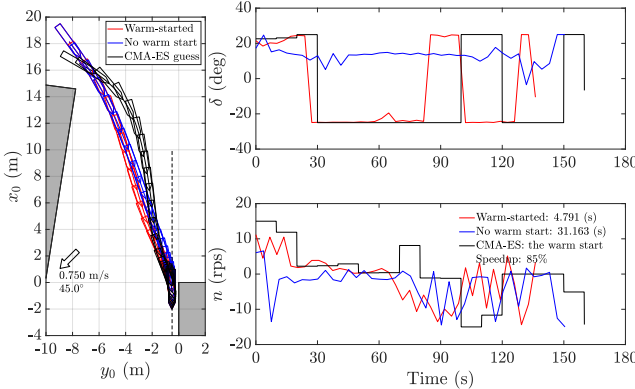


Fig. 7: Case M2: summary and optimal control trajectories, $V(\bar{t}_j) = 0.75$ m/s, $\chi(\bar{t}_j) = 45^\circ$, $u(\bar{t}_j) = 0.24$ m/s, $\psi(\bar{t}_j) = 4\pi/5$, with 4.791 s calculation time.

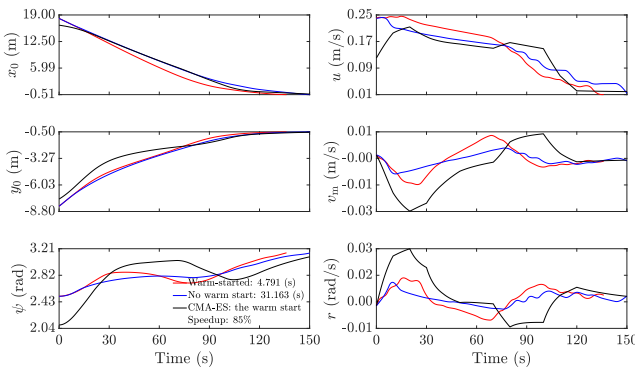


Fig. 8: Case M2: optimal state trajectories, $V(\bar{t}_j) = 0.75$ m/s, $\chi(\bar{t}_j) = 45^\circ$, $u(\bar{t}_j) = 0.24$ m/s, $\psi(\bar{t}_j) = 4\pi/5$, with 4.791 s calculation time.

Because now the initial surge velocity is doubled (0.24 m/s; equivalent to 4.86 knots for the full scale ship), the time t_f that is required to reach the desired docking states \mathbf{x}_{fin} is shorter, even when the initial position is farther. The solution from the warm-started SO-TP gives a shorter t_f than that without warm start. This is as expected because the OCP is a minimum-time problem.

The warm-started SO-TP also converged to a feasible and collision-free solution in a relatively faster computational time than that without warm start. This M2 case demonstrates that the warm start is still applicable to a situation which initial states are different (norm $L = 1.03$) and with wind disturbance.

4.1.3. Case M3: Wind Blows to the Berth + Closer Initial States

In contrast to the previous case M2, in case M3 the initial position of the ship is closer to the berth and the initial yaw angle is sharper against the berth. Such initial condition limits the free area for the ship to maneuver. In this case, the wind speed is 0.5 m/s and it blows from at 225 degree quarterly to the berth. The resulting optimal control and state trajectories for this case are visualized in Fig. 9 and Fig. 10.

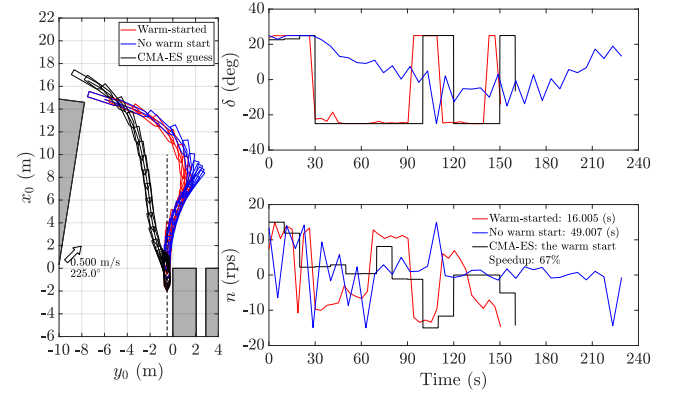


Fig. 9: Case M3: summary and optimal control trajectories, $V(\bar{t}_j) = 0.50$ m/s, $\chi(\bar{t}_j) = 225^\circ$, $u(\bar{t}_j) = 0.24$ m/s, $\psi(\bar{t}_j) = 3\pi/5$, with 16.005 s calculation time.

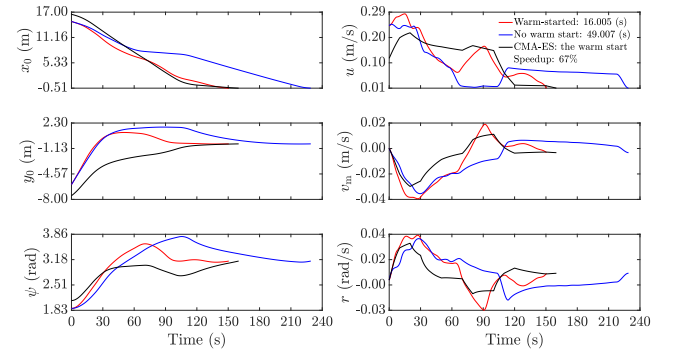


Fig. 10: Case M3: optimal state trajectories, $V(\bar{t}_j) = 0.50$ m/s, $\chi(\bar{t}_j) = 225^\circ$, $u(\bar{t}_j) = 0.24$ m/s, $\psi(\bar{t}_j) = 3\pi/5$, with 16.005 s calculation time.

It can be seen that now the problem becomes quite difficult for the ship to reach the desired docking states \mathbf{x}_{fin} from the given initial states because the ship is expected to do a sharp turn in such a relatively narrow area. This is implied by the longer computational time that is required for the SO-TP to converge. Nevertheless, the warm start gives a considerable 67% computational speedup.

Similar to the previous case, t_f is shorter than that of the warm start, this is because the initial surge velocity is doubled; small thrust from the propeller can give more momentum for the ship to do a sharp turn. From Fig. 9, one can also observe that the SO-TP without warm start results in t_f that is much longer than the warm-started SO-TP.

Keen readers may find it interesting to see the same tendency that the resulting optimal δ trajectory is similar to the warm start. This shows that the thrust from the propeller contributes significantly to the overall maneuverability of the ship. An intuitive explanation to this tendency is that the warm start for δ gives the objective function value that is in the neighborhood of the curvature of the interpolation (9d) and quadrature equality constraints (9e), while that for n is far from the curvature of the equality constraints.

4.1.4. Case M4: Wind Blows Away from the Berth + Large Deviation

Suppose now the ship arrives at an entry location with initial yaw angle that is quite different from that of the warm start: parallel to the berth. The ship also arrives at a surge velocity 0.36 m/s; three times of that of the warm start: equivalent to 7.26 knots for the full scale ship. In this case, the wind blows at 0.75 m/s away from the berth. Such condition is very different from the warm start with norm $L = 2.06$. The resulting optimal control and state trajectories are shown in Fig. 11 and Fig. 12.

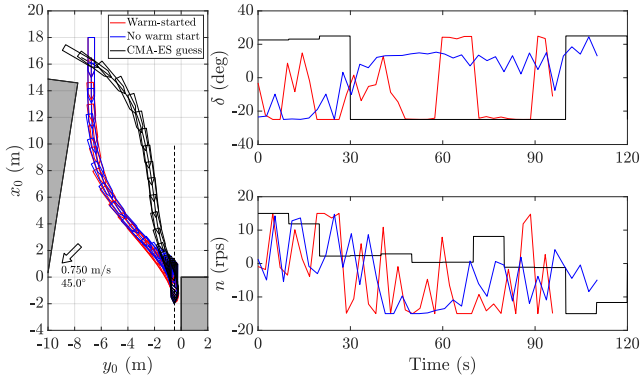


Fig. 11: Case M4: summary and optimal control trajectories, $V(\bar{t}_j) = 0.75$ m/s, $\chi(\bar{t}_j) = 45^\circ$, $u(\bar{t}_j) = 0.36$ m/s, $\psi(\bar{t}_j) = \pi$, with 17.211 s calculation time.

Despite the large difference of the initial states from the warm start, the warm-started SO-TP still gives a faster computational time than that without warm start: 55% speedup. This means that the warm start is still applicable to speed up the computation, even for a situation that is very much different from that when obtaining the warm start.

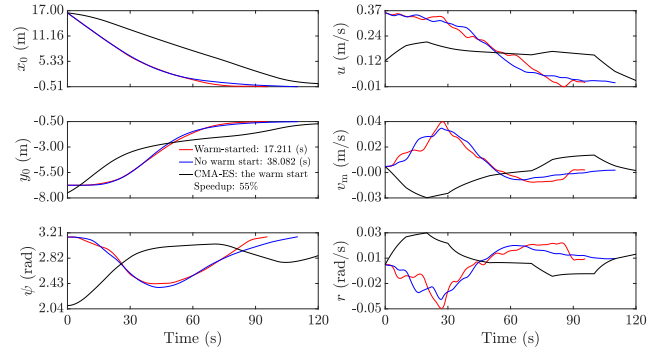


Fig. 12: Case M4: optimal state trajectories, $V(\bar{t}_j) = 0.75$ m/s, $\chi(\bar{t}_j) = 45^\circ$, $u(\bar{t}_j) = 0.36$ m/s, $\psi(\bar{t}_j) = \pi$, with 17.211 s calculation time.

To conclude this subsection about the first evaluation matter, the readers now must have a good grasp of the applicability of one almost-globally optimum solution from the Off-TP to warm start the SO-TP for various different scenarios. The resulting trajectories are guaranteed to be collision-free and satisfy the dynamics of the system.

4.2. Additional Trial Cases

As to further show the effect of warm start in the computational time and performance of the SO-TP (adhere to the second evaluation matter), 10 additional cases (A1 to A10) are also considered (see Table 2). The same offline solution from the Off-TP is used to warm-start the SO-TP. Note that A9 and A10 are the cases when the ship starts the docking operation from the East (positive y_0 axis), while the rest of the cases (M1 to A8) are from the West. For the sake of demonstration, these additional cases are chosen arbitrarily, with norm of the initial states L varies between 0 to 2.3.

The effect of warm start is evaluated based on the the computational time and the resulting t_f . The summary of these additional trial cases along with the main cases is presented in Table 3. It can be seen that the warm start by the Off-TP gives a significant reduction in the computational time. As a comparison, the average computational time of the SO-TP with warm start is 13.819 s while that without warm start is 63.644 s. The warm start by just one almost-globally optimum solution from the Off-TP gives an average of 71% computational time speedup. In addition, since the OCP is a kind of minimum-time problem, the warm-started SO-TP gives a shorter t_f for almost all of the cases.

4.3. The Necessity for the Off-TP

In adherence to the last evaluation matter, the authors tried to use the locally optimal solution for case M1 obtained by the SO-TP without warm start (use linear initial guess, see Fig. 5 and Fig. 6) to warm-start the SO-TP for the rest of the cases (M2 to A10). Following the previous subsection, the computational time and the resulting t_f are used as comparison between the two warm start methods. The summary is presented in Table 4.

From Table 4, almost half of the cases have one or more optimization variables that violate the constraints. It

Table 3

Comparison of the SO-TP: with and without warm start (16 GB RAM, 8-core processor laptop). See Fig. A.1 to Fig. A.3 in the appendix.

Case	Norm $L =$ $\sqrt{\sum_i^6 (d_i - 1)^2}$	$V(\bar{t}_j)$ (m/s)	$\chi(\bar{t}_j)$ (deg)	Warm start by Off-TP		No warm start (linear)		% Comp. speedup
	t_f (s)	Comp. time (s)	t_f (s)	Comp. time (s)				
M1	0.00	No wind	162.0	3.215	237.0	43.604		93%
M2	1.03	0.75 45	136.1	4.791	150.5	31.163		85%
M3	1.03	0.50 225	150.5	16.005	229.0	49.007		67%
M4	2.06	0.75 45	95.6	17.211	110.2	38.082		55%
A1	0.32	0.75 45	151.9	7.561	177.0	28.485		73%
A2	0.53	0.75 180	163.0	10.479	229.3	25.117		58%
A3	0.78	0.75 125	144.4	22.426	160.5	198.189		89%
A4	0.92	0.50 135	167.7	7.682	303.3	113.752		93%
A5	0.58	0.50 90	175.5	10.616	209.7	42.672		75%
A6	0.41	0.50 315	162.7	3.820	261.2	76.643		95%
A7	1.25	0.50 250	203.0	19.262	211.6	30.820		38%
A8	1.51	0.50 90	137.3	14.532	153.7	92.010		84%
A9	2.24	0.75 0	180.5	24.787	209.1	44.245		44%
A10	2.31	0.50 45	212.0	30.284	184.6	72.277		58%
				AVG	13.819	AVG	63.644	71%

Table 4

Comparison of the SO-TP: warm-started by the Off-TP and warm-started by the SO-TP for case M1 with no warm start.

Case	Warm start by Off-TP				Warm start by SO-TP (M1, no warm start)				% Comp. speedup
	t_f (s)	Feasi- ble?	Constraint violation	Comp. time (s)	t_f (s)	Feasi- ble?	Constraint violation	Comp. time (s)	
M2	136.1	Yes	2.4E – 11	4.791	227.4	No	4.4E – 3	35.397	-
M3	150.5	Yes	1.5E – 11	16.005	239.5	Yes	1.2E – 11	17.066	6%
M4	95.6	Yes	1.7E – 11	17.211	292.4	No	6.1E – 3	117.571	-
A1	151.9	Yes	4.5E – 12	7.561	223.4	No	1.5E – 3	47.334	-
A2	163.0	Yes	2.2E – 11	10.479	239.1	Yes	9.3E – 11	14.181	26%
A3	144.4	Yes	1.2E – 7	22.426	200.1	No	1.7E – 3	202.903	-
A4	167.7	Yes	2.0E – 11	7.682	245.3	No	1.8E – 3	64.192	-
A5	175.5	Yes	1.7E – 10	10.616	254.3	No	2.2E – 3	170.028	-
A6	162.7	Yes	1.2E – 12	3.820	252.1	Yes	3.2E – 12	13.859	72%
A7	203.0	Yes	8.3E – 11	19.262	235.5	Yes	9.7E – 11	16.038	-20%
A8	137.3	Yes	5.2E – 12	14.532	232.7	No	4.2E – 2	33.967	-
A9	180.5	Yes	4.3E – 11	24.787	252.3	Yes	8.6E – 10	44.485	44%
A10	212.0	Yes	9.0E – 11	30.284	316.5	Yes	2.8E – 10	84.974	64%

is apparent that the solution from the SO-TP without warm start should not be used even as an initial guess for different problems as it can not dictate the search to a feasible solution. This situation implies the nonlinear nature of the NLP and that the SQP requires a good "starting point" for the search to converge to a feasible solution.

Therefore, to maximize the potential of the SO-TP, a good initial guess is important to warm start the optimization. Such initial guess can readily be obtained by the Off-TP which applicability to many situations have been demonstrated in subsection 4.1 and summarized in Table 3. To conclude this subsection, the Off-TP and SO-TP should be implemented together so that both can exploit their respective advantages to compromise each other's disadvantages.

5. Concluding Remarks

This article demonstrates a warm-started semionline trajectory planner (SO-TP) that is applicable for underactuated vessel, able to guarantee that the feasible trajectory is safe, and able to consider the wind dynamics up to some extent. It has been shown that significant reduction in the computational time of the SO-TP can be achieved with the solution from the offline trajectory planner (Off-TP) as a warm start. The versatility of just one solution from the Off-TP to warm-start the SO-TP for many different scenarios have also been demonstrated.

However, there is no guarantee that the warm start or any initial guess will result in a feasible solution or computational time speedup. The underactuation and the restricted harbor area greatly limit the existence of the feasible solutions, which is reasonable. This suggests that the presence of a feedback controller is necessary, so that practically when the trajectory planner fails, the previously obtained trajectory can still be used as the set point for the feedback controller (Martinsen et al., 2020).

The readers may still be wondering about the semionline (not in real time) nature of the computational time. Again, the authors would like to underline that this is due to the nonlinearity and the underactuation of the system; result in a harder NLP and more mathematical function evaluations. Nevertheless, frequently replanning the reference trajectory may lead to the instability of the feedback controller. Since the average computational time from the 14 trial cases shown in this article is less than 30 seconds, for a full scale ship, it is relatively fast. Consider this as a contribution to realize an online trajectory planner for an underactuated vessel in the future.

As an idea for the next work, one can construct a database of offline solution by the Off-TP from several initial states and wind conditions. These offline solutions can be organized into a grid system from which the SO-TP will choose one best offline solution to be used as its warm start. This is why the authors introduced the norm L in the discussion: to measure the deviation of the initial states from that of the offline solution, i.e., chose one offline solution that gives the smallest L as a warm start. By doing this, given by the demonstrated versatility of one solution from the Off-TP to speed up the SO-TP for many different situations, it is more likely that the average computational time can be further shortened. This will be implemented in the near future in an actual experiment with the model scale.

Even though not related to autonomous ship, as an example of the implementation of the warm-started SO-TP, a shipmaster can use the resulting trajectory as a guide when maneuvering the ship to dock. Moreover, the feasibility status from the SO-TP can be used as a qualitative measure as to whether the shipmaster should proceed to dock or not. In this sense, when the SO-TP can not give a feasible solution, within the accuracy of the mathematical model of the ship, it is safe to say that the ship can not reach the desired docking states from the given initial states under a certain condition by herself.

Declaration of Competing Interests

The authors declare that they have no known competing financial interests or personal relationships that could have appeared to influence the work reported in this paper.

Acknowledgment

This study was supported by a Grant-in-Aid for Scientific Research from the Japan Society for Promotion of Science (JSPS KAKENHI Grant #19K04858).

CRediT authorship contribution statement

Dimas M. Rachman: Conceptualization, Methodology, Software, Writing - original draft. **Atsuo Maki:** Conceptualization, Supervision, Writing - review & editing. **Yoshiki Miyauchi:** Writing - review & editing. **Naoya Umeda:** Supervision, Funding acquisition.

A. Appendix

Table A.1
Principal particulars of Esso Osaka 1/108 model scale.

Parameters	Measurement
Length between perpendiculars L_{pp} (m)	3.000
Breadth B (m)	0.489
Draught d (m)	0.201
Longitudinal center of gravity x_G (m)	0.095
Mass m (kg)	245.091
Block coefficient C_b	0.831

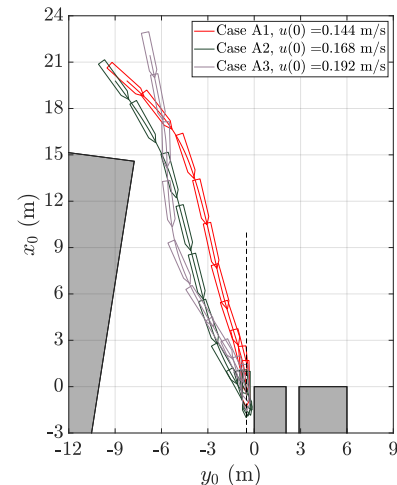


Fig. A.1: Result from the warm-started SO-TP: case A1 to case A3.

References

Auger, A., Hansen, N., 2005. A restart CMA evolution strategy with increasing population size, in: 2005 IEEE congress on evolutionary computation, IEEE. pp. 1769–1776.

Betts, J.T., 2010. Practical Methods for Optimal Control and Estimation Using Nonlinear Programming. Second ed., Society for Industrial and Applied Mathematics. URL: <https://pubs.siam.org/doi/abs/10.1137/1.9780898718577>, doi:10.1137/1.9780898718577, arXiv:<https://pubs.siam.org/doi/pdf/10.1137/1.9780898718577>.

Bitar, G., Martinsen, A.B., Lekkas, A.M., Breivik, M., 2020. Trajectory planning and control for automatic docking of ASVs with full-scale experiments. IFAC-PapersOnLine 53, 14488–14494. URL: <https://www.sciencedirect.com/science/article/pii/S2405896320318632>, doi:<https://doi.org/10.1016/j.ifacol.2020.12.1451>. 21st IFAC World Congress.

Boggs, P.T., Tolle, J.W., 1995. Sequential quadratic programming. Acta Numerica 4, 1–51. doi:10.1017/S0962492900002518.

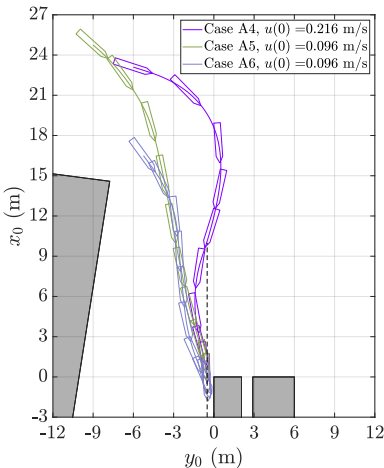


Fig. A.2: Result from the warm-started SO-TP: case A4 to case A6.

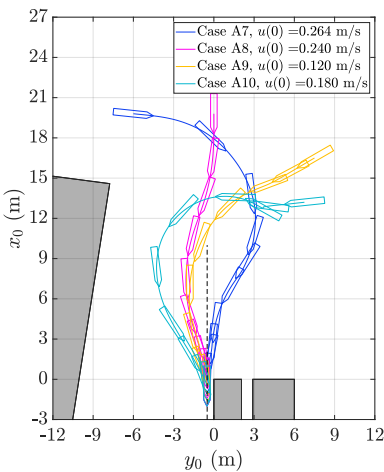


Fig. A.3: Result from the warm-started SO-TP: case A7 to case A10.

Forsgren, A., 2006. On warm starts for interior methods, in: Ceragioli, F., Dontchev, A., Futura, H., Marti, K., Pandolfi, L. (Eds.), *System Modeling and Optimization*, Springer US, Boston, MA. pp. 51–66.

Fujiwara, T., Ueno, M., Nimura, T., 1998. Estimation of wind forces and moments acting on ships. *Journal of the Society of Naval Architects of Japan*, 77–90doi:10.2534/jjasnae1968.1998.77.

Han, S., Wang, Y., Wang, L., He, H., 2021. Automatic berthing for an underactuated unmanned surface vehicle: A real-time motion planning approach. *Ocean Engineering* 235, 109352. URL: <https://www.sciencedirect.com/science/article/pii/S002980182100768X>, doi:<https://doi.org/10.1016/j.oceaneng.2021.109352>.

Hansen, N., Müller, S.D., Koumoutsakos, P., 2003. Reducing the time complexity of the derandomized evolution strategy with covariance matrix adaptation (CMA-ES). *Evolutionary Computation* 11, 1–18. doi:[10.1162/106365603321828970](https://doi.org/10.1162/106365603321828970).

Hormann, K., Agathos, A., 2001. The point in polygon problem for arbitrary polygons. *Computational Geometry* 20, 131–144. URL: <https://www.sciencedirect.com/science/article/pii/S0925772101000128>, doi:[https://doi.org/10.1016/S0925-7721\(01\)00012-8](https://doi.org/10.1016/S0925-7721(01)00012-8).

Kitagawa, Y., Tsukada, Y., Miyazaki, H., 2015. A study on mathematical models of propeller and rudder under maneuvering with propeller reverse rotation. *Conference Proceedings The Japan Society of Naval Architects and Ocean Engineers* 20, 117–120.

Liao, Y., Jia, Z., Zhang, W., Jia, Q., Li, Y., 2019. Layered berthing method and experiment of unmanned surface vehicle based on multiple constraints analysis. *Applied Ocean Research* 86, 47–60. URL: <https://www.sciencedirect.com/science/article/pii/S0141118718304759>, doi:<https://doi.org/10.1016/j.apor.2019.02.003>.

Maki, A., Akimoto, Y., Umeda, N., 2021. Application of optimal control theory based on the evolution strategy (CMA-ES) to automatic berthing (part: 2). *Journal of Marine Science and Technology* 26, 835–845. URL: <https://doi.org/10.1007/s00773-020-00774-x>, doi:[10.1007/s00773-020-00774-x](https://doi.org/10.1007/s00773-020-00774-x).

Maki, A., Sakamoto, N., Akimoto, Y., Nishikawa, H., Umeda, N., 2020. Application of optimal control theory based on the evolution strategy (CMA-ES) to automatic berthing. *Journal of Marine Science and Technology* 25, 221–233.

Martinsen, A.B., Bitar, G., Lekkas, A.M., Gros, S., 2020. Optimization-based automatic docking and berthing of ASVs using exteroceptive sensors: Theory and experiments. *IEEE Access* 8, 204974–204986. doi:[10.1109/ACCESS.2020.3037171](https://doi.org/10.1109/ACCESS.2020.3037171).

Martinsen, A.B., Lekkas, A.M., Gros, S., 2019. Autonomous docking using direct optimal control. *IFAC-PapersOnLine* 52, 97–102. URL: <https://www.sciencedirect.com/science/article/pii/S2405896319321755>, doi:<https://doi.org/10.1016/j.ifacol.2019.12.290>. 12th IFAC Conference on Control Applications in Marine Systems, Robotics, and Vehicles CAMS 2019.

Miyauchi, Y., Maki, A., Umeda, N., Rachman, D.M., Akimoto, Y., 2021a. System parameter exploration of ship maneuvering model for automatic docking / berthing using CMA-ES. [arXiv:2111.06124](https://arxiv.org/abs/2111.06124). manuscript submitted for publication.

Miyauchi, Y., Sawada, R., Akimoto, Y., Umeda, N., Maki, A., 2021b. Optimization on planning of trajectory and control of autonomous berthing and unberthing for the realistic port geometry. URL: <https://arxiv.org/abs/2106.02459>, arXiv:2106.02459. manuscript submitted for publication.

Mizuno, N., Uchida, Y., Okazaki, T., 2015. Quasi real-time optimal control scheme for automatic berthing. *IFAC-PapersOnLine* 48, 305–312. URL: <https://www.sciencedirect.com/science/article/pii/S2405896315021886>, doi:<https://doi.org/10.1016/j.ifacol.2015.10.297>. 10th IFAC Conference on Manoeuvring and Control of Marine Craft MCMC 2015.

Press, W.H., Teukolsky, S.A., Vetterling, W.T., Flannery, B.P., 1992. *Numerical Recipes in C*. Second ed., Cambridge University Press, Cambridge, USA.

Sakamoto, N., Akimoto, Y., 2017. Modified box constraint handling for the covariance matrix adaptation evolution strategy, in: *Proceedings of the Genetic and Evolutionary Computation Conference Companion*, pp. 183–184.

Shouji, K., Ohtsu, K., Mizoguchi, S., 1992. An automatic berthing study by optimal control techniques. *IFAC Proceedings Volumes* 25, 185–194.

Vagale, A., Ouchekh, R., Bye, R.T., Osen, O.L., Fossen, T.I., 2021. Path planning and collision avoidance for autonomous surface vehicles I: a review. *Journal of Marine Science and Technology*, 1–15URL: <https://link.springer.com/article/10.1007/s00773-020-00787-6>, doi:[10.1007/s00773-020-00787-6](https://doi.org/10.1007/s00773-020-00787-6).

Yasukawa, H., Yoshimura, Y., 2014. Introduction of MMG standard method for ship maneuvering predictions. *Journal of Marine Science and Technology* 20, 37–52. doi:[10.1007/s00773-014-0293-y](https://doi.org/10.1007/s00773-014-0293-y).

Yoshimura, Y., Nakao, I., Ishibashi, A., 2009. Unified mathematical model for ocean and harbour manoeuvring, *International Conference on Marine Simulation and Ship Maneuverability*. pp. 116–124. URL: <http://hdl.handle.net/2115/42969>.

Zhou, C., Gu, S., Wen, Y., Du, Z., Xiao, C., Huang, L., Zhu, M., 2020. The review unmanned surface vehicle path planning: Based on multi-modality constraint. *Ocean Engineering* 200, 107043. URL: <https://www.sciencedirect.com/science/article/pii/S0029801820301177>, doi:<https://doi.org/10.1016/j.oceaneng.2020.107043>.